Thrust Enhancement of Wave-driven Unmanned Surface Vehicle by using Asymmetric Foil

Yan Gao[1,2], Lyucheng Xie[1,2] and Tin Lun Lam[1,2,†], *Senior Member, IEEE*

***Abstract*— In the Wave-driven unmanned surface vehicles (WUSVs), oscillating-foils are the most straightforward and widely used wave energy conversion mechanism. In this paper, a kind of novel asymmetric foil is proposed, which improves the wave energy-converting efficiency to provide a more significant thrust in every wave cycle. We break down the movement of the foils in the wave and build the corresponding kinetic model to analyze their working effectiveness numerically. Through computational fluid dynamic (CFD) simulations, we determine the optimal values of critical parameters of the foils, which are suitable for a wide range of wave conditions. The thrust enhancement of the asymmetric foil is verified in both CFD simulations and hydrodynamic experiments, and the result shows a similar enhancement trend. Comparing with the traditional symmetric foil, our asymmetric foil can provide at least 13.75% more thrust to the WUSVs.**

I. INTRODUCTION

In recent years, the wave-driven unmanned surface vehicle (WUSV) has been widely considered by researchers [1]–[4]. WUSV is an unmanned vehicle that sails on the sea surface by merely utilizing wave energy as its driving power [5]. Many researchers choose to use oscillating foils to absorb wave energy and convert it into the propulsion of WUSVs, as previous studies have pointed out that oscillating foils are invested as unsteady thrusters which augment ship's overall propulsion in waves [6]. Oscillating foils, at optimum conditions, can achieve high thrust level and efficiency, supported by extensive experimental evidence and theoretical analysis [7], [8]. In WUSVs, the movement of the foils is usually passive or semi-passive, while the foils are fixed on the vehicle's body or the separate propeller by the axis. There exist several kinds of angle limiting mechanisms to limit the maximum pitching angle of the foils. As shown in Fig. 1. The working principle of foils is that when the vehicle rises and falls with the waves, it will generate a vertical relative flow to the foils, resulting in the foils pitching down and up, by which the foils convert the wave energy into forwarding propulsion force.

There are four groups of governing parameters that determine the propulsion performance of the oscillating foils: environmental parameter, geometric parameter, kinematic parameter, and performance parameter [9]. Geometric parameters are the most important and widely studied parameters because environmental parameters are uncontrollable and kinematic parameters and performance parameters are actually determined by geometric parameters. This means that the shape of the foil is the core of its propulsion performance, which decides its thrust force in every wave cycle. One of the previous researches simulates the propulsion performance of NACA type foil numerically using the spectral difference (SD) method [10]. The results indicate that relative thin foils show superior propulsion performance, on the effect of foil thickness based Reynolds numbers. Another research established a scaling law for the thrust of a foil and found that low aspect-ratio foils can improve thrust force produced by the foils when they start from rest [11]. From the bionic point of view, some researchers began to study on the foil's flexibility. One of the methods is to treat the foil as a non-extensible thin line, ignoring the foil's thickness and shape [12]. In incompressible and laminar flows, moderate flexibility is beneficial to symmetry preservation in the wake, while excessive flexibility can trigger symmetry-breaking. In addition, one of the researches further studied the propulsion performance of bionic fin-like foils [13].

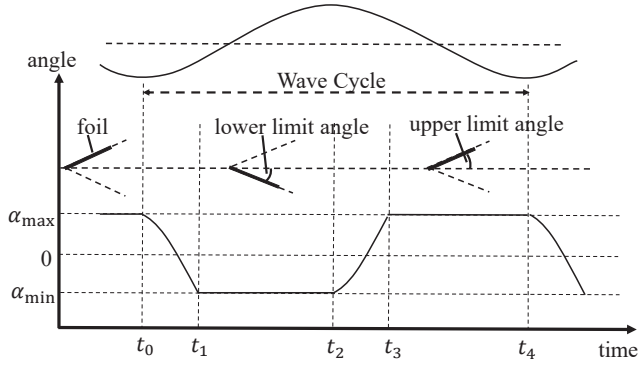

Fig. 1. The view of the movement of a passive-motion foil in one wave cycle and the change of the angle between foil and horizontal.

Most previous studies focused on parameters of the foil including the chord length, the maximum thickness, the span length, the aspect ratio, and some special bionic parameters. These studies are all based on the foils with symmetrical cross-section shapes, including rectangle, ellipse, and teardrop shapes. In this paper, we propose one kind of asymmetric foil with passive motion (no any actuation) used on WUSVs for the first time. The experiment results show that our asymmetric foil can provide at least 13.75% more thrust force than the traditional foil under the same wave condition.

This paper is organized as follows, Section II describes

Research supported by the Opening Project of Guangdong Provincial Key Lab of Robotics and Intelligent System.

[1]The Chinese University of Hong Kong, Shenzhen, 518172, China.

[2]Shenzhen Institute of Artificial Intelligence and Robotics for Society.

[†]The corresponding author is Tin Lun Lam, Email: tllam@cuhk.edu.cn

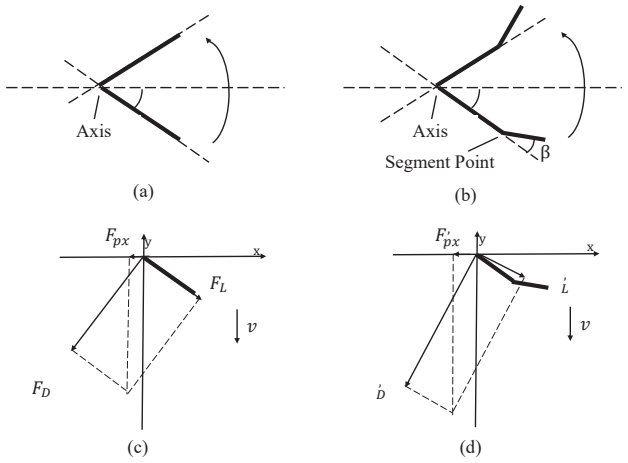

Fig. 2. (a) Structure movement of traditional foil. (b) Structure movement of asymmetric foil. (c) Force analysis of traditional foil in time interval T_u [t_1,t_2]. (d) Force analysis of asymmetric foil in T_u [t_1,t_2].

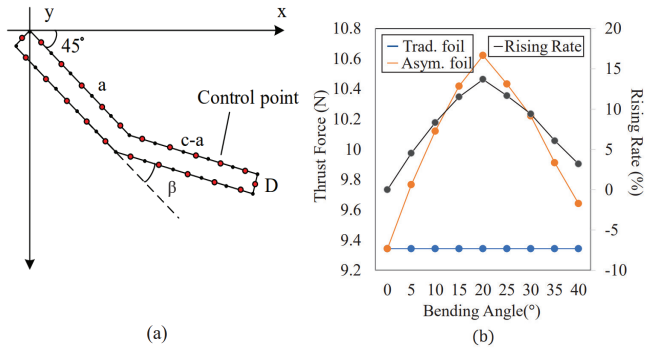

Fig. 3. (a) Asymmetric Foil Control Points. (b) Thrust force rising rate between traditional foil and asymmetric foil with different bending angle at the lower limit angle 45 degrees, flow speed 5 cm/s.

the different foils and their dynamic model. Section III describes the CFD simulations with the parameters optimization method, the corresponding hydrodynamic experiments are presented in Section IV. Both Sections include the relative experiments, results, and analysis. The conclusion follows in Section V.

II. DESIGN OF ASYMMETRIC FOIL

As the foils are fixed on the body or the separate propeller of the WUSV by the axis, the vehicle's heaving motions in the wave cause a vertical relative flow to the foils, which drives the foils pitching down and up. For foils, as shown in Fig. 1, the movement in every wave cycle is composed of 5 steps: (1) initially at the up boundary where the angle between the foil and the horizontal is the upper limit angle and start to swing down at t_0; (2) swing and reach the down boundary at time t_1; (3) hold at this position until start to swing up at time t_2; (4) swing and reach the up boundary at time t_3; (5) hold at this position until swing down again at time t_4.

The critical factor affecting the foil propulsion performance is that how the foils respond to the flow in time intervals T_u $[t_1, t_2]$ and T_l $[t_3, t_4]$. The asymmetric foil we proposed in this paper is a rigid two-part foil, as shown in Fig. 2(b). The segment point separate the foil into two parts and the external angle of the two parts is the bending angle β. The limiting angle is the max rotation angle which determines the boundary.

A. Traditional Foil

Fig. 2(c)(d) shows the force on the traditional foil and asymmetric foil in T_u $[t_1, t_2]$. The velocity v is the relative velocity of the water to the foil. The angle α is the direction of horizontal relative to the foil. The direction of the form drag forces F_D and the friction drag force F_L generated by a single foil are also shown. The form drag forces F_D is perpendicular to the foil, while the friction drag force F_L is in the same direction of foil. Refer to [14], they can be expressed as Eq. 1.

$$\begin{cases} F_D = 0.5\rho v^2 S_w C_D(\alpha) \\ F_L = 0.5\rho v^2 S_w C_L(\alpha) \end{cases} \tag{1}$$

where ρ denotes the water density, S_w denotes the projected area with respect to xz plane, $C_D(\alpha)$ and $C_L(\alpha)$ are the form drag coefficient and friction drag coefficient respectively, and they are both the function of angle of attack. We suppose that the flow is incompressible and inviscid. C_L is 0 and C_D is 2 [15]. We can draw the driving force F_{px} in the foil reference frame:

$$\begin{aligned} F_{px} &= -F_D \sin\alpha + F_L \cos\alpha \\ &= -\rho v^2 S_w \sin\alpha \end{aligned} \tag{2}$$

B. Asymmetric Foil

For asymmetric foils, we can solve for forces by using the panel method [16]. Using the condition that the velocity of the fluid must be tangent to the surface of the object, a set of equations can be obtained which can be used to get the intensity distribution. We choose appropriate control points with proper spacing on the object's surface and make sections of the object through control points. The object's surface is replaced by several panels while assuming that the intensity distribution is uniform on one panel. We put the point source and the point vortex on the control point which reflect the interaction between the fluid and object. The point source intensity of panel j is q_j and the point vortex intensity of panel j is γ_j.

For panel j, its velocity potential of source Φ_j and velocity potential of vortex Ψ_j can be expressed as Eq. 3.

$$\begin{cases} \Phi_j = \dfrac{q_j}{2\pi} \displaystyle\int_{S_i} \ln \sqrt{(x-x_j)^2 + (y-y_j)^2}\, dS_i \\ \Psi_j = \dfrac{\gamma_j}{2\pi} \displaystyle\int_{S_i} \arctan \dfrac{y-y_j}{x-x_j}\, dS_i \end{cases} \tag{3}$$

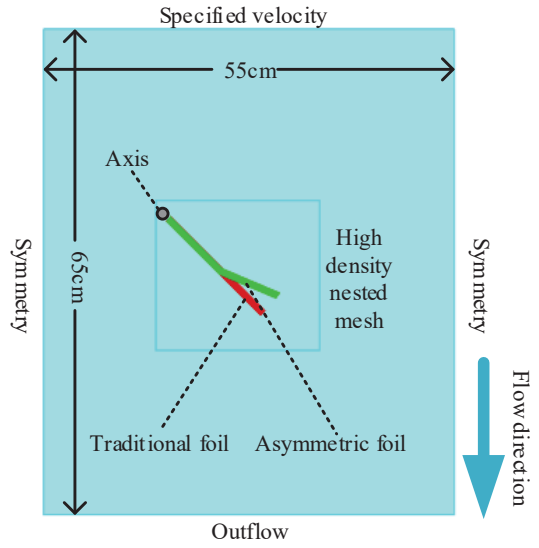

Fig. 4. Fluid region and foils setup of the simulations. The size of the fluid region: X-55 cm, Y-65 cm, Z-100 cm. The boundaries of the fluid region are set as follows: XMIN-Symmetry, XMAX-Symmetry, YMIN-Outflow, YMAX-specified velocity, ZMIN-Symmetry, ZMAX-Symmetry.

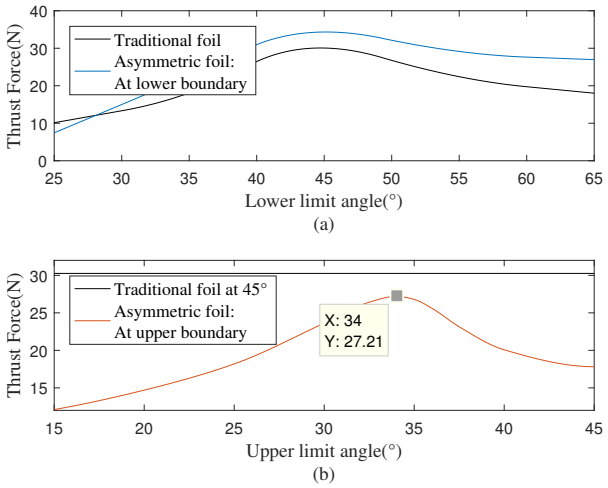

Fig. 5. (a) Thrust force at different limit angles (the upper and lower limit angles of traditional foil, and lower limit angle of asymmetric foil), with a constant flow speed 40 m/s. The randomly selected parameters of asymmetric foil in this simulation: segment point 10 cm (10/18); bending angle 22 degrees. (b) Thrust force of the asymmetric foil at different upper limit angles (less than 45 degrees), with a constant flow speed 40 cm/s. The optimized parameter pair: segment point 11 cm, bending angle 25 degrees.

where S_j is the area of panel j. Because the normal velocities from both point source velocity potential and point vortex velocity potential on the surface of panel i is 0, Eq. 4 can be built, where v_∞ is the inflow velocity and k is the number of the panel.

$$\begin{cases} v_\infty \dfrac{\partial x}{\partial n_i} + \displaystyle\sum_{j=1}^{k} \frac{\partial \Phi_j}{\partial n_i} = 0, \ \ i = 1, ..., k \\ \displaystyle\sum_{i=1}^{k} \frac{\partial \Phi}{\partial n_i} = 0, \ \ i = 1, ..., k \end{cases} \tag{4}$$

According to the intensity distribution, the tangential velocity v_{Si} on the panel i are expressed as:

$$v_{Si} = v_\infty \frac{\partial x}{\partial S_i} + \sum_{j=1}^{k} \frac{\partial \Phi_j}{\partial S_i} + \sum_{j=1}^{k} \frac{\partial \Psi_j}{\partial S_i} \tag{5}$$

Accoding to Kutta-Joukowski condition,

$$v_{S1} = v_{Sk} \tag{6}$$

q_i, γ_i, and v_{Si} can be solved from Eqs. 3 to 6.

Pressure distribution p_i can be calculated using Bernoulli's principle. F_{px} can be expressed as:

$$F_{px} = \int_{S_i} p_i \cos\theta_i \, dS_i \tag{7}$$

Where θ_i is the angle between the direction of S_i and the horizontal. It can be solved numerically by substituting the assumed parameters. Fig. 3(a) shows the choices of control points in asymmetric foil. According to Eq. 2, F_{px} of traditional foil reaches a maximum when $\alpha = 45°$ and thus we set $\alpha = 45°$ for asymmetric foil here too.

To preliminarily prove the thrust enhancement effect of our asymmetric foil at this lower boundary, we divide the asymmetric foil into 10 equal parts by 11 control points on each side. Other parameters chosen for asymmetric foil: $v = 5\ cm/s$, chord length $c = 10\ cm$, $a = 5\ m$, thickness $D = 1\ cm$, span length $L = 100\ cm$. The traditional foil has the same chord length, span length, and thickness. The thrust force of traditional foil and asymmetric foil and the rising rate are shown in Fig. 3(b). The thrust force of asymmetric foil is bigger than that of traditional foil at different bending angles we chose. We can find that 20° is a better bending angle to make the foils to produce the most thrust force with the parameters we chose.

III. THRUST FORCE SIMULATION

To verify the thrust enhancement effect of our asymmetric foil in Section II and determine its three critical parameters in a proper order: lower limit angle, segment shape (including segment point and bending angle), and upper limit angle, we designed the corresponding CFD simulations using the software FLOW-3D [17]. The thrust performance difference between the asymmetric foil we proposed and the traditional foil is compared under the same wave conditions.

A. CFD simulation setup

As we introduced, the vehicle's heaving motions in the wave cause a vertical relative water flow to the foils, which drives the foils pitching down and up. In our simulations, traditional foil and asymmetric foil have the same basic specifications: chord length is 18 cm, thickness is 1 cm, and span length is 100 cm. The foils are placed in a rectangular fluid region, as shown in Fig. 4. To keep the original shape of the foils in the *FAVOR* rending system of FLOW-3D

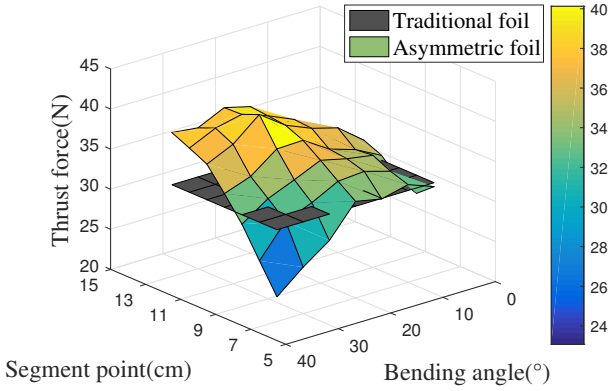

Fig. 6. Thrust force of the asymmetric foil with different parameter pairs (segment point and bending angle) at the lower limit angle 45 degrees, with a constant flow speed 40 cm/s.

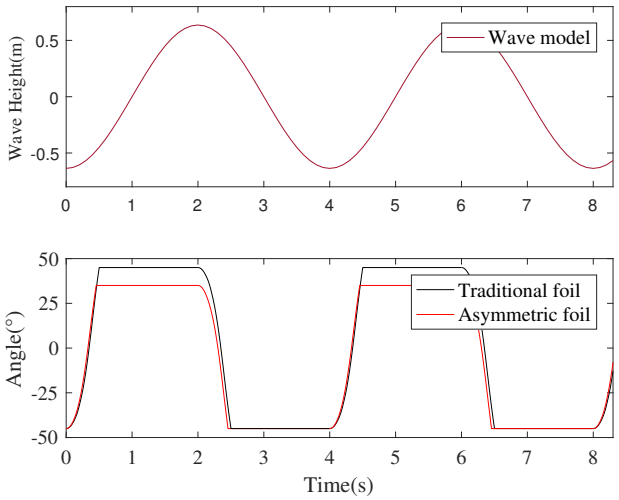

Fig. 7. Foils' rotation in a standard wave with amplitude 1.2 m and fixed-point wave period 4 s. Traditional foil: upper/lower limit angle 45 degrees; Asymmetric foil: upper limit angle 34 degrees, lower limit angle 45 degrees, segment point 11 cm, bending angle 25 degrees.

and the accuracy of the simulation results, a high-density mesh is nested in the motion area of the foils, which is constituted of 0.1 cm $\times$ 0.1 cm Cartesian grid [18]. The grid number in the Z direction is always 1, which is a semi-3D simulation, but the span length will be calculated in the pressure solver. Since we don't know the best segment shape of the asymmetric foil, we randomly choose two parameters which seem reasonable in this part: the segment point is 10 cm (the distance between the segment point and the rotation axis), and the bending angle is 22 degrees. The optimal values of these two parameters will be found in the following parts. The position of the black spot is the axis of the foil's rotation, and the upper boundary is the direction of fluid flowing in. For the turbulence model, we choose the common renormalized group (RNG) model [19]. The boundaries of the fluid region are shown in Fig. 4. The "Symmetry" boundary condition in FLOW-3D means that applying a zero-gradient condition at the boundary as well as a zero velocity condition normal to the boundary.

B. The lower limit angle

In every wave cycle, the main time intervals for the foils to generate thrust force are T_u ($[t_1, t_2]$) and T_l ($[t_3, t_4]$) at the limit angle positions. Before we find the two best segment shape of the asymmetric foil, we need to determine the value of the lower limit angle of the foils first. It should be noted that the upper and lower limit angles of traditional foil are the same in gravity-free condition, while that of asymmetric foil are different due to its asymmetric structure. The gravity-free condition means there is a gravity counteracting device, like NACA-structure foils [20] or springs, or no gravity considered. We set the relative flow to the foils as a uniform flow at a velocity of 40 cm/s, which is common in the seas [21], and the total simulation time is 6 seconds to reach the steady-state.

Through different limit angle simulations, we found that the best limiting angle (the upper and lower limit angles of traditional foil, and lower limit angle of asymmetric foil) to make the foils to produce the most thrust force is about 45 degrees, as shown in Fig. 5(a). We don't need an exact lower limit angle of the asymmetric foil because subsequent segment shape optimization will maximize the thrust. What's more, the thrust change rate of the asymmetric foils is faster at a lower angle and slower at a higher angle than the traditional foil in the simulation interval because of its asymmetric structure.

C. Bending angle and segment point of asymmetric foil at the lower limit angle

With this lower limit angle, the randomly selected segment shape of asymmetric foil can be optimized: segment point and bending angle. Using the same simulation method, the foils with different parameter pairs in the flow are simulated. The simulation results are shown in Fig. 6.

The black plane is the contrast data of the traditional foil. We can see that not all the asymmetric foils perform better than the traditional foil, such as low segment point and large bending angle (the bent section of the foil is long and the angle between the two sections of the foil is small, like 6/18 and 35 degrees). Finally, the best thrust enhancement effect can reach 31.76% ((39.87N/30.26N)-1) at the lower limit angle with the parameter pair: the segment point is 11 cm, and the bending angle is 25 degrees.

D. The optimal upper limit angle of asymmetric foil

Due to the special shape of the asymmetric foil, a smaller upper limit angle (less than 45 degrees) is needed to compensate for the loss of thrust force. With the same method, we get the simulation results as shown in Fig. 5(b). From the results, we can see the best upper limit angle is 34 degrees with a minimum thrust loss of 10.08% (27.21N/30.26N-1). So far, we have determined all the parameters of the asymmetric foil: segment point is 11 cm, bending angle is 25 degrees,

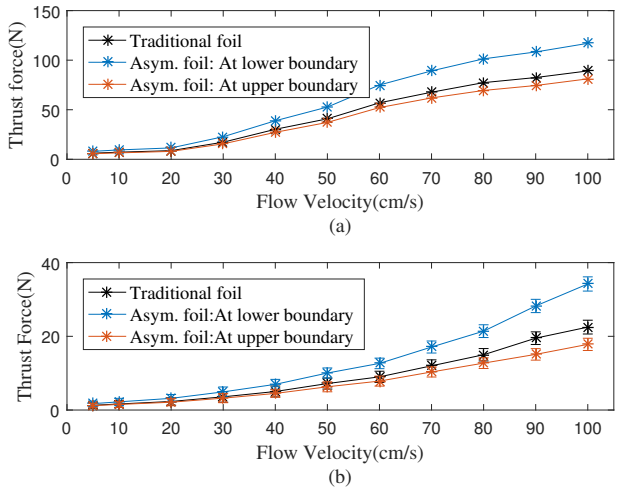

Fig. 8. (a) Simulation: Foils' thrust force in different flow velocities. Traditional foil: upper/lower limit angle 45 degrees; Asymmetric foil: upper limit angle 34 degrees, lower limit angle 45 degrees, segment point 11 cm, bending angle 25 degrees. (b) Experiment: Foils' thrust force with different flow velocities at upper(pitching up)/lower(pitching down) limit angles, mean value of 10 experiments' data.

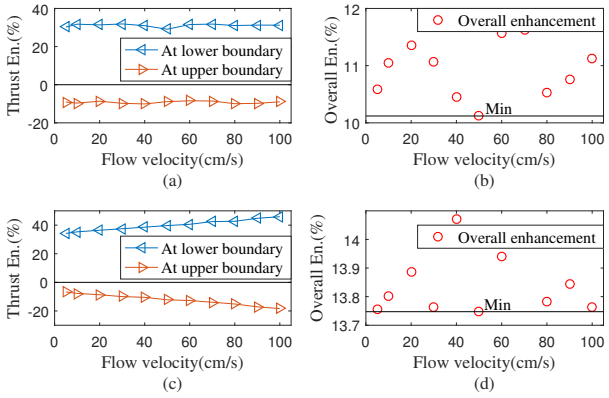

Fig. 9. (a) (b) Simulation: Thrust enhancement/loss percentage of the asymmetric foil at lower/upper limit angle in different flow velocities, with upper limit angle 34 degrees, lower limit angle 45 degrees, segment point 11 cm, bending angle 25 degrees. Overall thrust enhancement effect is calculated by Eq. 9. (c)(d) Experiments: Thrust enhancement/loss percentage of our asymmetric foil at upper(pitching up)/lower(pitching down) limit angles and its overall thrust enhancement effect.

lower limit angle is 45 degrees, and upper limit angle is 34 degrees.

E. Pitching motion simulation in standard wave

After determining all the parameters of the asymmetric foil, we need to simulate its pitching motion in the wave to obtain the time intervals T_l and T_u. We selected a wave case which is common in the seas [21]: the wave amplitude A is 1.2m, and the fixed-point wave period T_w is 4 seconds. Under this wave condition, the wave function and relative flow in the vertical direction on the foil is as follow:

$$\begin{cases} y(t) = -0.6\cos(\dfrac{\pi t}{2}) \\ v(t) = 0.3\pi\sin(\dfrac{\pi t}{2}) \end{cases} \tag{8}$$

The density of the foils is $2.0\times10^3 kg/m^3$, which is about the density of glass fiber reinforced plastics (FRP). From the simulation result Fig. 7, we get the values of time intervals T_u^T ($[t_1, t_2]$) and T_l^T ($[t_3, t_4]$) of traditional foil are both 1.49 seconds (74.5% of half wave), while those are 1.53 seconds (T_u^A,76.5% of half wave) and 1.54 seconds (T_l^A, 77% of half wave) of asymmetric foil. Due to the asymmetric structure and smaller rotation angle of the asymmetric foil, the time intervals of different foils follow that: $T_u^A \approx T_l^A > T_u^T = T_l^T$.

F. Thrust enhancement effect

In waves, the relative flow to the foil is variable rather than a single uniform flow, as shown in Fig. 7. To obtain the overall thrust enhancement effect of asymmetric foil in the waves, we also need to obtain its thrust enhancement/loss effect under various relative flows. The asymmetric foil's working effect is simulated in the flow velocity range of 1 m/s, and the result is shown in Fig. 8(a).

Finally, the thrust enhancement/loss effect of the asymmetric foil under various relative flows can be obtained, shown in Fig.9 (a) (b). The overall thrust enhancement effect E_o is 10.12%, according to the Eq. 9.

$$\begin{aligned} E_o &= \frac{\int_{T_l^A}(1+E_t)dt + \int_{T_u^A}(1+L_t)dt}{\int_{T_l^T}1dt + \int_{T_u^T}1dt} - 1 \\ &\geq \frac{\int_{T_l^T}(1+E_t+1+L_T)dt}{2T_l^T} - 1 \\ &\geq \min\frac{E_t+L_t}{2}, t\in T_l^T \end{aligned} \tag{9}$$

Where E_t/L_t are the thrust enhancement/loss percentage at time t. It can be verified that as long as the wave condition meets the following: $\frac{2\pi A}{T} \leq 1$ (the maximum relative flow velocity is in the range of our simulations), the thrust enhancement of asymmetric foil is always effective.

IV. Hydrodynamic Experiments

We built a propeller prototype, which could carry different kinds of foils, and an experimental framework to test the thrust enhancement effect of our asymmetric foil. The thrust test experiments were carried out in a water tank.

A. Experimental setup

Compared with a single large foil, we choose to make a Wave Glider type propeller [1], which is easy to fix and operate, as shown in Fig. 10. The propeller is composed of one backbone and six pairs of foils. The foils (both traditional foils and asymmetric foils) are dismountable though the connection part. The angle limiting mechanism is implemented by the connection part and backbone with the arc holes, which are different for two kinds of foils. The full prototype

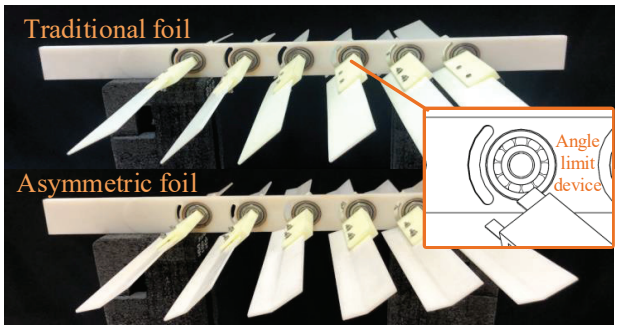

Fig. 10. Propeller prototypes made by 3D printing with density around 1 g/cm^3 (material density 1.25 $g/cm^3\times$ fill rate 80%). Upper side: propeller with the tradition foils, whose span length 20 cm, chord length 4 cm, thickness 0.2 cm, upper/lower limit angle 45 degrees; Lower side: propeller with our asymmetric foils, whose segment point 2.4 cm (4 cm $\times$ 11/18), bending angle 25 degrees, lower limit angle 45 degrees, upper limit angle 34 degrees.

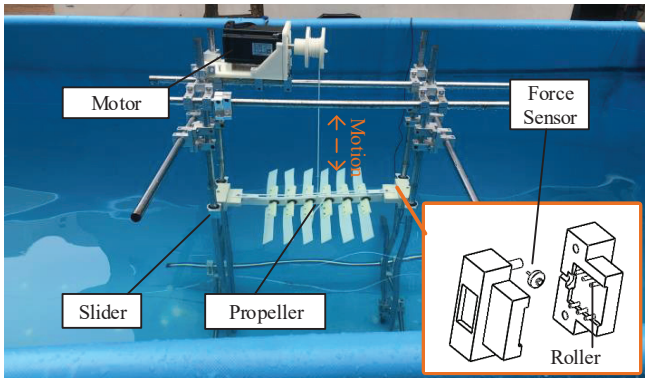

Fig. 11. The heavy sliders can freely move on the sliding rails and a motor is used to drives the propeller up/down. The head and tail of the propeller are inserted into the thrust detection devices. A force sensor is placed in the edge of the device, which will touch the head of the propeller during the experiments. Several rollers with bearing are used to offset the friction caused by the propeller's slight slip. The experiment framework is placed in a water poll, with the water elevation about 1.3 m.

is 57 cm long and 42 cm wide, including the 20 cm long foils, with the distance between every pair of neighbor foils is 5.5 cm. The detailed parameters are shown in Table I.

TABLE I
PARAMETERS OF THE PROTOTYPE

	Length	Width	Thickness
Backbone	37 cm	4 cm	1 cm
Trad. foil	20 cm	4 cm	0.2 cm
Asym. Foil	20 cm	4 cm	0.2 cm

The propeller and the corresponding thrust force detection equipment are placed in a water pool with scale: 4 m length $\times$ 2 m width $\times$ 1.5 m height. A thin rope suspends the prototype on a wire wheel controlled by an electric motor, as shown in Fig. 11. The propeller's head and tail are inserted into the sliders equipped with a force sensor and several rollers to reduce the friction.

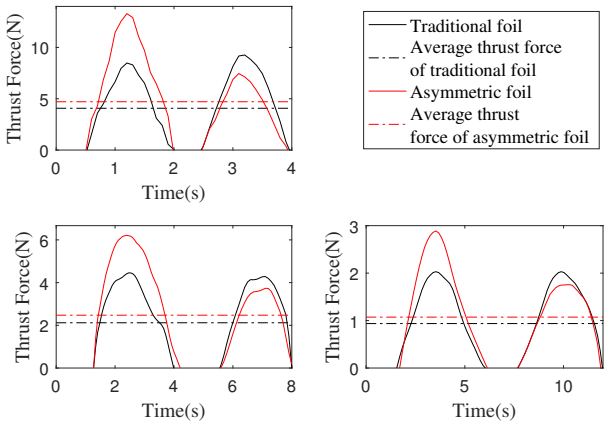

Fig. 12. Foils' thrust force in a complete wave period. Wave amplitude is 0.8 m and wave periods are 4 s, 8 s, and 12 s. The thrust enhancement effects: 15.59% $((4.7084N/4.0732N)-1)$, 16.77% $((2.4748N/2.1194N)-1)$, and 14.49% $((1.0727N/0.9369N)-1)$.

B. Thrust enhancement experiments in constant flows

The method we used to create the relative flow was to use an electric motor to pull the propeller, rather than to directly create water flow like some previous researches [22]. For each relative flow velocity, we take the average thrust force of ten times experiments, as shown in Fig. 8(b).

Unlike the simulation results, the thrust enhancement/loss effect of asymmetric foil increases with the increase of flow velocity, which may be caused by the RNG model's inaccuracy in high-speed flow simulation. The following derivations are based on the experimental value. According to Eq. 9, the overall thrust enhancement effect E_o in the wave is 13.75% ($E_o \geq min(E_t - L_t)/2 = 0.1375$), as shown in Fig. 9(c)(d).

C. Thrust enhancement verification in waves

We use a motor to simulate the wave with amplitude A of 0.8m and the wave period T_w of 4 seconds, 8 seconds, and 12 seconds. Fig. 12 shows the thrust force of the foils in a complete wave period. The average thrust forces of asymmetric foil and traditional foil in each wave condition are also shown, and the thrust enhancement effects are 15.59%, 16.77%, and 14.49%, all larger than $E_o = 13.75\%$.

V. CONCLUSIONS AND FUTURE WORK

In this work, one kind of asymmetric oscillating-foil is proposed, which can significantly improve the thrust force of the propeller provided to the WUSVs. Its thrust enhancement effect is verified through the numeric method, CFD simulations, and hydrodynamic experiments. The experimental results show that the asymmetric foil can enhance the thrust of WUSVs at least 13.75% in a broad range of wave conditions. As the foil can not be deformed, it will cause a thrust loss at the upper limit angle. In future research, we will improve the asymmetric foil so that it can be deformed to fit both the upper and lower limit angles, which makes it reach a better thrust enhancement effect.

REFERENCES

[1] R. Hine, S. Willcox, G. Hine, and T. Richardson, "The wave glider: A wave-powered autonomous marine vehicle," in *OCEANS 2009*, pp. 1–6, 2009.

[2] P. Johnston and M. Poole, "Marine surveillance capabilities of the autonaut wave-propelled unmanned surface vessel (usv)," in *OCEANS 2017 - Aberdeen*, pp. 1–46, 2017.

[3] J. Manley and S. Willcox, "The wave glider: A persistent platform for ocean science," in *OCEANS'10 IEEE SYDNEY*, pp. 1–5, 2010.

[4] B. Tian, J. Yu, A. Zhang, F. Zhang, Z. Chen, and K. Sun, "Dynamics analysis of wave-driven unmanned surface vehicle in longitudinal profile," in *OCEANS 2014 - TAIPEI*, pp. 1–6, 2014.

[5] P. Liu, Y. Su, F. Liu, Y. Liu, J. Zhang, and S. Huang, "A utilizing efficiency estimation method for wave-driven unmanned surface vehicle," *Ocean Engineering*, vol. 164, pp. 650–660, 2018.

[6] E. Filippas and K. Belibassakis, "Hydrodynamic analysis of flapping-foil thrusters operating beneath the free surface and in waves," *Engineering Analysis with Boundary Elements*, vol. 41, pp. 47–59, 2014.

[7] M. S. Triantafyllou, G. S. Triantafyllou, and D. K. P. Yue, "Hydrodynamics of fishlike swimming," *Annual Review of Fluid Mechanics*, vol. 32, no. 1, pp. 33–53, 2000.

[8] K. von Ellenrieder, K. Parker, and J. Soria, "Fluid mechanics of flapping wings," *Experimental Thermal and Fluid Science*, vol. 32, no. 8, pp. 1578–1589, 2008.

[9] X. Wu, X. Zhang, X. Tian, X. Li, and W. Lu, "A review on fluid dynamics of flapping foils," *Ocean Engineering*, vol. 195, p. 106712, 2020.

[10] M. Yu, Z. Wang, and H. Hu, "High fidelity numerical simulation of airfoil thickness and kinematics effects on flapping airfoil propulsion," *Journal of Fluids and Structures*, vol. 42, pp. 166–186, 2013.

[11] J. Lee, Y.-J. Park, K.-J. Cho, D. Kim, and H.-Y. Kim, "Hydrodynamic advantages of a low aspect-ratio flapping foil," *Journal of Fluids and Structures*, vol. 71, pp. 70–77, 2017.

[12] X. Zhu, G. He, and X. Zhang, "Numerical study on hydrodynamic effect of flexibility in a self-propelled plunging foil," *Computers & Fluids*, vol. 97, pp. 1–20, 2014.

[13] G. K. Politis and V. Tsarsitalidis, "Simulating biomimetic (flapping foil) flows for comprehension, reverse engineering and design," in *First International Symposium on Marine Propulsors*, 2009.

[14] P. J. Pritchard and J. W. Mitchell, *Fox and McDonald's introduction to fluid mechanics*. John Wiley & Sons, 2016.

[15] J. Haibo, C. Shuliang, and C. Zhongqing, "Lift and drag coefficients of flow around a flat plate at hi gh attack angle.[j]," *Chines Journal of Applied Mechanics*, vol. 5, pp. 518–520, 2011.

[16] J. D. Anderson and J. Wendt, *Computational fluid dynamics*, vol. 206. Springer, 1995.

[17] C. Hirt and B. Nichols, "Flow-3d users manual," *Flow Science Inc*, vol. 107, 1988.

[18] T. Ye, R. Mittal, H. Udaykumar, and W. Shyy, "An accurate cartesian grid method for viscous incompressible flows with complex immersed boundaries," *Journal of Computational Physics*, vol. 156, no. 2, pp. 209–240, 1999.

[19] V. Yakhot and S. A. Orszag, "Renormalization group analysis of turbulence. i. basic theory," *Journal of scientific computing*, vol. 1, no. 1, pp. 3–51, 1986.

[20] B. Monnier, A. Naguib, and M. Koochesfahani, "Influence of structural flexibility on the wake vortex pattern of airfoils undergoing harmonic pitch oscillation," *Experiments in Fluids*, vol. 56, no. 4, p. 80, 2015.

[21] C. Zheng, H. Zhuang, X. Li, and X. Li, "Wind energy and wave energy resources assessment in the east china sea and south china sea," *Science China Technological Sciences*, vol. 55, no. 1, pp. 163–173, 2012.

[22] K. Lua, S. Dash, T. Lim, and K. Yeo, "On the thrust performance of a flapping two-dimensional elliptic airfoil in a forward flight," *Journal of Fluids and Structures*, vol. 66, pp. 91–109, 2016.